1521-009X/49/9/760–769$35.00
DRUG METABOLISM AND DISPOSITION

https://doi.org/10.1124/dmd.121.000474
Drug Metab Dispos 49:760–769, September 2021

Characterization of Hepatic UDP-Glucuronosyltransferase Enzyme Abundance-Activity Correlations and Population Variability Using a Proteomics Approach and Comparison with Cytochrome P450 Enzymes[S]

Ryan H. Takahashi,[1] William F. Forrest, Alexander D. Smith, Justine Badee,[2] NaHong Qiu, Stephan Schmidt, Abby C. Collier, Neil Parrott, and Stephen Fowler

Department of Drug Metabolism and Pharmacokinetics (R.H.T.) and Department of OMNI Bioinformatics (W.F.F.), Genentech, Inc., South San Francisco, California; Department of Pharmaceutics, Center for Pharmacometrics and Systems Pharmacology, University of Florida at Lake Nona, Orlando, Florida (J.B., S.S.); Pharmaceutical Research and Early Development, Roche Innovation Centre Basel, F. Hoffmann-La Roche Ltd., Basel, Switzerland (N.Q., N.P., S.F.); Faculty of Pharmaceutical Sciences, The University of British Columbia, Vancouver, British Columbia, Canada (A.D.S., A.C.C.)

Received March 18, 2020; accepted Jun 24, 2021

ABSTRACT

The expression of ten major drug-metabolizing UDP-glucuronosyltransferase (UGT) enzymes in a panel of 130 human hepatic microsomal samples was measured using a liquid chromatography-tandem mass spectrometry–based approach. Simultaneously, ten cytochromes P450 and P450 reductase were also measured, and activity-expression relationships were assessed for comparison. The resulting data sets demonstrated that, with the exception of UGT2B17, 10th to 90th percentiles of UGT expression spanned 3- to 8-fold ranges. These ranges were small relative to ranges of reported mean UGT enzyme expression across different laboratories. We tested correlation of UGT expression with enzymatic activities using selective probe substrates. A high degree of abundance-activity correlation (Spearman's rank correlation coefficient > 0.6) was observed for UGT1As (1A1, 3, 4, 6) and cytochromes P450. In contrast, protein abundance and activity did not correlate strongly for UGT1A9 and UGT2B enzymes (2B4, 7, 10, 15, and 17). Protein abundance was strongly correlated for UGTs 2B7, 2B10, and 2B15. We suggest a number of factors may contribute to these differences including incomplete selectivity of probe substrates, correlated expression of these UGT2B isoforms, and the impact of splice and polymorphic variants on the peptides used in proteomics analysis, and exemplify this in the case of UGT2B10. Extensive correlation analyses identified important criteria for validating the fidelity of proteomics and enzymatic activity approaches for assessing UGT variability, population differences, and ontogenetic changes.

SIGNIFICANCE STATEMENT

Protein expression data allow detailed assessment of interindividual variability and enzyme ontogeny. This study has observed that expression and enzyme activity are well correlated for hepatic UGT1A enzymes and cytochromes P450. However, for the UGT2B family, caution is advised when assuming correlation of expression and activity as is often done in physiologically based pharmacokinetic modeling. This can be due to incomplete probe substrate specificities, but may also be related to presence of inactive UGT protein materials and the effect of splicing variations.

Introduction

The liver is often the most important organ for drug clearance given its high delivery of systemic blood, large organ mass, and high expression of metabolizing enzymes (Williams et al., 2004; Cerny, 2016). The enzymes of highest interest, due to their predominant role in metabolizing small molecule drugs, belong to the cytochrome P450 (P450) and UDP-glucuronosyltransferase (UGT) families (Cerny, 2016). There has been an apparent movement in the chemistries of candidate drug molecules away from primarily P450-mediated clearance and toward other enzymes (Argikar et al., 2016; Cerny, 2016). Thus, it is likely that UGT-mediated conjugation will be more frequently encountered in candidate drug molecules, potentially reducing drug-drug interaction liabilities due to lower time-dependent inhibition and induction risks, but also requiring better understanding of these enzymes to enable in vitro metabolism characterization and prediction of in vivo outcomes.

Heterogeneity in hepatic enzyme expression between individuals can contribute to variability in drug pharmacokinetics and can cause risk of underexposure or overexposure to a new drug or its metabolites in

This work was partially funded by the National Sciences and Engineering Council of Canada [Grant 17-003808].

None of the authors has any conflict of interest to declare with respect to this study.

[1]Current affiliation: Denali Therapeutics, South San Francisco, California.

[2]Current affiliation: Department of PK Sciences, Novartis Institutes for BioMedical Research, Basel, Switzerland.

https://dx.doi.org/10.1124/dmd.121.000474.

[S] This article has supplemental material available at dmd.aspetjournals.org.

ABBREVIATIONS: HLM, human liver microsomes; IVIVE, in vitro-in vivo extrapolation; LC-MS/MS, liquid chromatography-tandem mass spectrometry; P450, cytochrome P450; PBPK, physiologically based pharmacokinetic; QC, quality control; rs, Spearman's rank correlation coefficient; SDC, sodium deoxycholate; SIL, stable isotope–labeled;SNP, Single Nucleotide Polymorphism; SRM, selected reaction monitoring; UGT, UDP-glucuronosyltransferase.

some individuals. This may result in lower drug efficacy or higher toxicity, especially for narrow therapeutic index drugs. Examples for UGT-cleared drugs that were recognized to have high interindividual variabilities are UGT2B10-metabolized RO5263397 (Fowler et al., 2015) and UGT2B17-metabolized MK-7246 (Wang et al., 2012). In vitro-in vivo extrapolation (IVIVE) embedded within physiologically based pharmacokinetic (PBPK) models is widely employed to predict a drug's pharmacokinetics and variability within a given population (Rowland et al., 2011). IVIVE relies on the assumption that enzyme abundance is predictive of in vivo activity, and population variability in enzyme abundance is a major contributor to projected in vivo clearance variability (Howgate et al., 2006). This IVIVE approach has been developed for P450 isoforms (Proctor et al., 2004), and PBPK models have been successfully verified for many P450-cleared drugs. The IVIVE approach is less well established for UGTs (Jones et al., 2015), for which (compared with P450s) fewer enzyme-selective probe substrates have been studied and over a shorter period of time. Recently, Docci et al. (2020) developed PBPK models for four UGT substrates, using available clinical data to overcome gaps in IVIVE. Their work also highlighted gaps and uncertainties in UGT abundance data, which currently limit IVIVE and PBPK modeling for UGT substrates.

Quantification of enzymes in human tissue samples is typically performed by measuring enzymatic activities or protein concentration/expression. Measurement of both, using the same panel of samples, enables cross-comparison of the methodologies and enhances confidence when these parameters are strongly correlated. When UGT activities for a large number of individual donor liver microsomal samples were measured, population variability and enzyme activity development with age could be approximated (Badée et al., 2019a; Liu et al., 2020). However, this approach consumes significant amounts of microsomal material and relies on the use of enzyme-selective probe substrates. Immunoblotting has historically been used for protein quantification, but this approach is resource-intensive, requiring each protein to be probed discretely. It can be limited by the availability of protein-specific antibodies and consumes large amounts of sample. As an alternate approach, LC-MS/MS monitoring and quantification of protein-specific surrogate peptides can be highly selective and sensitive, requires little material, and is amenable to multiplexing for simultaneously measuring several proteins (Prasad et al., 2017). This has led to its adoption for quantifying key drug-metabolizing enzymes and transport proteins and, in particular, has been applied to profiling large banks of individual donor samples (Bhatt and Prasad, 2018; Basit et al., 2020). With several laboratories having now reported LC-MS/MS quantifications of ADME proteins, it has become clear that differences exist in the methodologies employed and the expression levels reported (Achour et al., 2014a; Wegler et al., 2017; Achour et al., 2018). Whereas bioanalysis of new chemical entities or their metabolites follow stringent criteria for validation, there is still discussion on what constitutes best practice for proteomics approaches (Prasad et al., 2019).

In the current study, we quantified ten UGTs, encompassing the major drug-metabolizing isoforms, in a collection of human liver microsome samples using a LC-MS/MS–based proteomics approach. The methods here built upon previously reported approaches and focused on enhancing tryptic peptide recoveries, normalizing for interbatch variabilities, monitoring multiple peptides, and verifying the linearity via mixed human liver microsome (HLM) samples. The expression determinations were corroborated by comparing with enzymatic activities measured using probe substrates. The major hepatic drug-metabolizing P450s were simultaneously monitored in these studies, which enabled us to compare and contrast observations for the less-studied UGTs with those for well characterized P450s. The resultant data sets provide a rich description of the interindividual differences in enzyme expression, activity, and the correlation of these properties.

Materials and Methods

Materials. Single-donor HLM were obtained from commercial sources. 108 single-donor lots were purchased from Sekisui XenoTech (Lenexa, KS), and twelve lots were purchased from Corning (Woburn, MA). HLM from ten single pediatric donors were provided by Abby C. Collier (University of British Columbia, Canada, Human Subjects Approval H14-0009). The 200-donor mixed gender pooled HLM used as a batch QC sample was purchased from Corning. All microsomes were kept stored at −80°C. Stable isotope–labeled (SIL) peptide standards with ^{13}C and ^{15}N C-terminal lysine or arginine were purchased from New England Peptide (Gardner, MA) and CPC Scientific (Sunnyvale, CA). Peptide standards were received from the vendor with certificates of analysis confirming >95% peptide purity and >99% isotopic purity by amino acid analysis, matrix-assisted laser desorption/ionization mass spectrometry, and high-performance liquid chromatography analysis. SIL peptides were stored at −20°C and dissolved in water:acetonitrile (70:30 v:v) containing 0.1% formic acid. Ammonium bicarbonate, CelLytic M, dithiothreitol, iodoacetamide, and trypsin (sequencing grade) were purchased from Sigma (St Louis, MO). All other reagents were of analytical quality or higher.

Sample Demographics. The donor samples in this study were not selected to reflect a specific population but rather to represent a large range of livers that were available from commercial providers and research institute HLM collections. There were 83 male donors and 47 female donors. Most were of Caucasian origin (95) with a small number of African American (20), Hispanic (9), and Asian (3) origin. Ethnicities for 3 donors were not available. Following on from research into the ontogeny of drug-metabolizing enzymes (Badée et al., 2019a; Badée et al., 2019b), the sample set was somewhat enriched with pediatric donors. The donors ranged in age from 0.04 to 79 years of age, with the following number of samples in each age group: 0–2 years, 18; 2–6 years, 8; 6–12 years, 9; 12–18 years, 7; 18–60 years, 70; and 60–80 years, 18.

Trypsin Digestion of HLM Samples. A standard in-solution trypsin digestion protocol was optimized and then employed for this study. To allow batch analysis, sample preparation was completed using a 96-well plate format. The base protocol mixed microsomal samples (40 μg total protein, nominal protein concentrations provided by vendors were used) and dithiothreitol (10 mM) in ammonium bicarbonate buffer (22.5 mM) in a sample volume of 80 μl. Proteins were denatured by heating to 60°C for 1 hour, then allowed to cool to room temperature. Iodoacetamide was added as a solution in ammonium bicarbonate buffer (final 15 mM) and allowed to alkylate cysteine residues over 30 minutes in the dark at room temperature. Trypsin, dissolved in 50 mM acetic acid, was added to bring final sample volumes to 100 μl, and the samples were incubated overnight covered at 37°C with shaking. At the end of the incubation, acetonitrile containing 2 pmol of $^{13}C^{15}N$-isotopically labeled synthetic peptide (internal standard) corresponding to each target protein was added to each sample. Samples were vortex mixed and centrifuged at 2,000×*g* at 4°C for 10 minutes. Supernatants were removed and concentrated under vacuum, and the residues were redissolved to ∼0.3× volume with water:acetonitrile (70:30) containing 0.1% formic acid.

To evaluate the effect of surfactant on trypsin digestion efficiency and peptide recoveries, detergents were added to the initial mixture of microsomes and dithiothreitol in buffer. The tested detergents were sodium deoxycholate (SDC), which was added dissolved in ammonium bicarbonate buffer to 10% (w/v); or CelLytic M, a commercial solution of proprietary detergents, which was added to 31.2% (by volume) or 62.5% (by volume). The trypsin amount providing optimal peptide generation was judged by completing digestions at 1:100, 1:50, and 1:20 trypsin:protein ratios in a single experiment. For each optimization condition (detergent or trypsin), triplicate digestions were completed with a single microsomal sample to evaluate the reproducibility of the digestion.

Batch analysis of the single-donor HLM was completed using the base protocol, with the following best-tested conditions for digestion efficiency: addition of CelLytic at 62.5% (by volume) for denaturation and trypsin at 1:50 (ratio to protein). In each batch of samples, 4–6 replicates of 200-donor pooled HLM were included to act as QC samples. The 130 single-donor HLM lots were prepared and analyzed in two analytical batches with each lot in singlicate and the QC sample in replicate.

LC-MS/MS Analysis. Trypsin digests were chromatographed on a Nexera ultra performance liquid chromatography system (Shimadzu, Kyoto, Japan) and analyzed by scheduled selected reaction monitoring (SRM) analysis with a QTRAP 5500 hybrid mass spectrometer operated using Analyst 1.5 software (Sciex, Framingham, MA). 10 μl of prepared sample, which contained tryptic digest of ~4 μg of total microsomal protein, was injected to the column. Separations were completed on an Omega Polar PS-C18, 100 × 2.1 mm, 1.6 μm particle size, analytical column (Phenomenex, Torrance, CA) with a constant flow rate of 0.65 ml/min of mobile phases (A) 0.1% formic acid in water and (B) 0.1% formic acid in acetonitrile with a gradient elution program. The program started at 5% B, which was held for 2 minutes, then the %B was increased to 15% at 26 minutes, 20% at 38 minutes, and 45% at 46 minutes. The column was then washed at 98% B for 4 minutes before re-equilibration for 4 minutes at 5% B. The total run time was 55 minutes.

Method creation, data acquisition, and processing were completed using Skyline software (MacLean et al., 2010). One peptide was used for each target protein for quantification with SRM transitions calculated by Skyline and confirmed in method development experiments. Doubly and triply charged precursor ions and three singly charged product ions were used to monitor each peptide (Supplemental Table 1). Optimal declustering potential and collision energies for each SRM transition were predicted by Skyline algorithms. In addition to SRMs for the quantifier peptide, at least one additional unique peptide from a distinct region of the protein was monitored as a qualifier peptide. To monitor all SRM transitions in a single sample injection and chromatographic run, each transition was scheduled for 3 minutes centered at the expected retention time for each peptide with a target scan time of 1 second.

Data were imported to Skyline for inspection and integration. Peak area ratios for the quantifier peptide were normalized to those of the corresponding SIL peptide and scaled to the amount of SIL added to calculate the protein amount in each sample. SIL standards were not obtained for qualifier peptides. The nominal concentrations provided by the vendor or calculated based on the reported amount provided for SIL peptides were used for calibration. The expression was expressed as pmol of protein determined from analysis per total microsomal protein that was added to the digestion. The microsomal protein amounts were based on vendor-reported concentrations and were not remeasured. In each batch, a 200-donor pooled HLM lot was digested in replicate and analyzed alongside the single-donor HLM. To account for batch effects, the observed response for each single-donor HLM were normalized to the mean response for the 200-donor pooled HLM for each enzyme in the same batch.

Linearity of Methods. HLM linearity standards were created by mixing single-donor HLM lots that had been characterized as having low and high expression. Six pairs of HLM lots were selected to span the ranges of protein expression for nine major drug-metabolizing enzymes (CYP1A2, 2B6, 2C9, 2D6, 3A4, UGT1A1, 1A4, 2B7, 2B15). For each pair, HLM were mixed at 1:0, 1:4, 2:3, 3:2, 4:1, and 0:1 volume ratios (low expression:high expression) maintaining a constant total protein concentration of 20 mg/ml, then, a 40 μg aliquot was taken and processed in the same manner as used for all single-donor HLM lots. Linearity plots were constructed by plotting SRM responses, normalized to SIL peptide, against the nominal concentrations (pmol mg^{-1}) using Prism v 8.0.1 (GraphPad Software, Inc., San Diego, CA), and linearity was judged based on the coefficient of determination for the fitted regression line.

Comparisons to Previous Reports of UGT Expression. Values from ten reports relating to LC-MS/MS–based quantification of UGTs in HLM have been compared in this study (Ohtsuki et al., 2011; Harbourt et al., 2012; Fallon et al., 2013; Achour et al., 2014b; Gröer et al., 2014; Sato et al., 2014; Margaillan et al., 2015; Yan et al., 2015; Nakamura et al., 2016; Bhatt et al., 2018). Most reports described analysis of panels of single-donor samples (n = 4–48). For comparison with the current study and for calculating interlaboratory range and variability, all samples were assumed to be drawn from the same human population, and the mean reported value for individual UGT isoforms represented each study.

Correlation with Enzyme Activities. P450 activities data were provided in microsomal lot characterization data sheets and used with permission from Sekisui XenoTech. UGT activities data were measured by monitoring the glucuronide metabolite formation of identified substrates using automated methods that have been previously described (Badée et al., 2019c). The UGT isoform-selective substrates were β-estradiol, chenodeoxycholic acid, trifluoperazine, 5-hydroxytryptophol, propofol, zidovudine, amitriptyline, oxazepam, and testosterone to characterize the activities of UGT1A1, 1A3, 1A4, 1A6, 1A9, 2B7, 2B10, 2B15, and 2B17, respectively (Badée et al., 2019b). In addition, glucuronide formation of UGT-metabolized drugs were monitored, namely raltegravir (UGT1A1), dolutegravir (UGT1A1), lamotrigine (UGT1A4), mycophenolic acid (UGT1A9), gemfibrozil (UGT2B4, UGT2B7), ketoprofen (UGT2B7; 1A3), and RO5263397 (UGT2B10). Where the same lot of single-donor HLM had measurements for expression and activities for an enzyme, association of the two parameters was tested by Spearman correlation.

Statistical Analyses. Expression measurements of P450s and UGTs were completed in two analytical batches. Each batch contained replicate measurements (n = 4 or 6), performed as discrete sample preparations and analyses, of pooled human liver microsomes (200 donors) as a QC sample and to enable interbatch normalization. Concentrations measured in batch 1 were not modified. Concentrations measured in batch 2 were adapted by multiplying each value for the individual HLM samples by a normalization factor, as follows:

$$Normalization\ factor = \frac{Mean\ measured\ enzyme\ concentration\ (Pooled\ HLM,\ Batch\ 1)}{Mean\ measured\ enzyme\ concentration\ (Pooled\ HLM,\ Batch\ 2)}$$

Measurement of UGT activities were completed in a separate laboratory than expression measurements as has been previously reported (Badée et al., 2019b). Matched single-donor HLM samples were used for expression versus activity comparisons. Expression and activities of the single-donor HLM did not follow Gaussian distribution, so nonparametric statistical assessment was used. Correlation analysis was performed using Spearman rank order correlation test with P values of t-statistics to assess correlations of data. Positive correlations with $rs > 0.4$ were described as strong when $rs \geq 0.6$ and moderate when $0.6 > rs > 0.4$. Linear regression analysis was carried out to assess the linearity of relationships and scatter of the data. Statistical analysis and graph generation was completed using R (version 4.0.0, R Core Team, 2020) and Prism version 8.1.2 (GraphPad Software, San Diego, CA).

Results

Method Optimization. In developing methods, key areas that were evaluated were peptide selection, trypsin digestion efficiency, and robustness of the mass spectrometric analysis.

Several expected peptides were chosen per target protein at the outset of method testing and monitored through method development and optimization experiments. Peptides that had been previously reported for quantitative analysis of UGTs or P450s were prioritized. Peptides were not used if they were not detected, showed poor peak shape, or showed reduced response when samples were reanalyzed 24–48 hours after initial analysis. The SIL peptide for the most promising peptide per protein was obtained by commercial custom synthesis and monitored as the primary quantifier peptide. Other peptides that remained after triage were maintained in the LC-MS/MS method as qualifier peptides.

Pooled HLM were digested in four digestion buffers and three trypsin-to-protein ratios in a single experiment. Each buffer and trypsin condition was performed with three replicates. The highest observed peptide:SIL ratios were recognized as the maximal recoveries of peptides to select the preferred sample digestion conditions (Supplemental Fig. 1). There was little difference observed when trypsin:protein ratio was increased from 1:100 to 1:50, but further increase to 1:20 introduced more variability in replicate samples. The use of surfactant is important to ensure solubilization of membrane-bound proteins or to provide access to proteins sequestered by a membrane layer; however, the addition of surfactant can inhibit the activity of trypsin. For P450s, there was little change observed when SDC or CelLytic detergent was added to the tryptic digestion. In contrast, the addition of SDC lead to ~4-fold increase of UGT peptides and CelLytic (added to 31.3% by volume) provided 5- to 9-fold increases in UGT peptides recovered. Peptide recoveries were higher with CelLytic than with inclusion of SDC, and therefore, it was used for all subsequent batch analyses. The

choice of a proprietary detergent mixture, CelLytic, was based on convenience and the potential to apply the proteomics method to hepatocyte samples in future.

Scheduled MRM successfully allowed all of the peptides to be monitored in a single analysis of each sample. The target cycle time was set as 1 second. The chromatographic run was 55 minutes per sample. When run times were shortened significantly from this, there were not enough scans to properly quantify some peaks.

Comparison of Quantifier and Qualifier Peptides. Each UGT and P450 was quantified using a surrogate peptide for which the SIL standard was obtained. During analysis, other protein-selective peptides were monitored as qualifier peptides. The MS response (peak area abundances) for the quantifier and qualifier peptides were compared during the method development with a set of seventeen samples that ranged in UGT and P450 abundances. If the peptides were equally recovered from the protein and analytically robust, peak areas were expected to correlate well. Good agreement between quantifier and qualifier peptides was seen for most proteins monitored in this study as judged by Spearman rank correlation (rs) of 0.80–0.99 (Table 1). Two exceptions with observed discordance for the monitored peptides were UGT1A3 and UGT2B10, which had low/no correlation (rs = 0.09 and 0.32, respectively). In the case of UGT1A3, the quantifier peptide (YLSIPTVFFLR) showed a dynamic range across the HLM samples, indicating it likely captured intersubject variability. In contrast, the qualifier peptide did not, potentially due to some isobaric background signal, and was therefore not used. For UGT2B10, the quantifier (ANVIATALAK) and qualifier peptides (DTFWLPFSQEQEILWAINDIIR and GHEVTVLASSASILFDPNDSSTLK) have been previously described by other laboratories (Achour et al., 2014b; Gröer et al., 2014). The peptide GHE … K was not considered ideal and was used as a qualifier without the SIL standard because it was long (24 amino acids), contained asparagine, which had potential to undergo deamidation, and contained the D67Y polymorphism site. In contrast, ANV … K is also present in human UGT2B11 and UGT2B28, although low interference from these proteins with UGT2B10 is expected in human liver microsomes, as discussed later. There was a strong correlation of ANV … K with GHE … K (rs = 0.96), but weak correlation with DTF … R (rs = 0.32), and weak correlation of GHE … K with DTF … R (rs = 0.37). A limitation in our UGT2B10 studies is that the final peptide selection was completed later in method development, and the full sample set was not available for measurements (n = 49 for expression analysis and n = 32 for enzymatic activity).

Native Protein Expression Linearity Assessment Using HLM. Six pairs of single-donor HLM were selected to represent the lowest and highest expressers of nine major drug-metabolizing enzymes, namely UGTs 1A1, 1A4, 2B7, and 2B15 as well as P450s 1A2, 2B6, 2C9, 2D6, and 3A4. These HLM pairs were mixed at six defined ratios to create mixed HLM samples that spanned the range of hepatic expression for these enzymes. Each mixed HLM sample was processed and analyzed with the same method that was applied to single-donor HLM. Linearity curves spanned large ranges of protein expression, ranging from 13.3-fold for UGT2B7 to 815-fold for CYP1A2, and linearity (coefficient of determination) ranged from 0.808–0.955 (Supplemental Fig. 1; Supplemental Table 2). There were no obvious dependences on enzyme or concentrations for scatter of residuals.

UGT and P450 Expression in HLM. The expression of UGTs and P450s in single-donor HLM (n = 130) and 200-donor pooled HLM are shown in Fig. 1. Large interindividual variability in expression was observed for most enzymes. The 10th and 90th percentiles were used to describe the characteristics of the population and avoid focusing on individual outliers (UGTs: Table 2; P450s: Supplemental Table 3). UGTs, other than UGT2B17, showed relatively small ranges in 10th to 90th percentile expression (3- to 8-fold). The largest 10th to 90th percentile range of all the studied enzymes was for UGT2B17 (79-fold range). However, this range is more reflective of the apparent bimodal distribution and cannot be compared directly with the largely monomodal distributions seen for other UGTs (Fig. 1). The UGT2B17 observations were consistent with those previously described by Bhatt et al. (2019), with low expression in samples from donors 12 years and younger, and a greater incidence of high expression in males than in females from donors older than 12 years. Other enzymes with non-Gaussian distributions in expression that tended toward bimodal were CYP2C19, CYP2D6, and CYP3A5, which have previously identified to be polymorphic, affecting expressed protein levels. Generally, the median expression for the single donors was similar to the 200-donor pooled lot (Table 2). Except for UGT2B17, the single-donor mean and the pooled-donor abundances differed by less than 50%. The difference for UGT2B17 was 2.1-fold.

The mean expression determined for each UGT in the panel of liver samples was compared with values found in literature (Fig. 2). Ten UGT datasets (Ohtsuki et al., 2011; Harbourt et al., 2012; Fallon et al., 2013; Achour et al., 2014b; Gröer et al., 2014; Sato et al., 2014; Margaillan et al., 2015; Yan et al., 2015; Nakamura et al., 2016; Bhatt et al., 2018) were used as comparators. The reported mean UGT expression levels ranged 10- to 100-fold, indicating large interlaboratory variabilities. Mean expression levels in this study were within the ranges of previously reported means for all of the enzymes, except UGT2B15 and UGT2B17. The UGT pie showing mean data from the current analysis showed the majority of hepatic UGT content being attributed to UGT1A1, 1A4, and 2B7 (Supplemental Fig. 2).

Correlation of UGT Expression Profiles. Correlation was tested in abundance versus abundance with pairwise comparisons of individual UGT isoforms. Visual representation of the correlation matrix is shown as Fig. 3. Strong protein expression correlations (Spearman correlation coefficient rs > 0.6) were observed between UGT2B7–2B10, UGT2B7–2B15, and UGT2B10-2B15. Correlations with 0.5 ≤ rs ≤ 0.6 were observed between the following pairs of UGTs: 1A4–2B4, 1A6–1A9, 1A6–2B10, 2B4-2B10, 2B4–2B15.

Association of Expression and Activities. HLM from pediatric (n = 43) and adult (n = 43) donors were incubated under optimized incubation conditions to assess the activity rates of hepatic UGTs using a panel of 16 in vitro UGT probe substrates and clinically used drugs, with each compound tested discretely (Badée et al., 2019b; Badée et al., 2019c). 108 HLM lots were characterized for P450 activities by the supplier (Sekisui Xenotech) using accepted chemical probes and monitoring the formation of isoform-selective metabolites. The Spearman correlation coefficients for the expected substrate reactions and matched enzyme expression are described in Table 3.

P450 probe substrate activities correlated strongly with the measured expressions (rs = 0.61–0.91; Table 3). Associations for CYP1A2, CYP2B6, CYP2C8, and CYP3A4/5 were determined using two substrates per enzyme and showed superior correlations using phenacetin (compared with ethoxyresorufin), bupropion (compared with (*S*)-mephenytoin), and amodiaquine (in comparison with paclitaxel), respectively, reflecting greater enzyme selectivity for these probe reactions. CYP3A4 expression correlated more strongly with testosterone 6β-hydroxylation (rs = 0.94) than with midazolam 1′-hydroxylation (rs = 0.84), presumably due to the involvement of CYP3A5 in metabolizing midazolam (Williams et al., 2002; Tseng et al., 2014). Indeed, correlation of CYP3A5 was higher with midazolam metabolism (rs = 0.55) than testosterone metabolism (rs = 0.43), although both correlations were substantially lower than those for CYP3A4 with these

TABLE 1

Spearman correlations for mass spectrometric responses (peak area abundances) of monitored quantifier and qualifier peptides for UGT enzymes

Protein Target	Quantifier Peptide	Qualifier Peptide(s)	Correlation	
			Sample *n*	Spearman rs
UGT1A1	DGAFYTLK[a,b,c,d,e]	GHEIVVLAPDASLYIR[d]	16	0.959
		TYPVPFQR[b,d,f]	17	0.838
		EVTVQDLLSSASVWLFR[g]	17	0.865
UGT1A3	YLSIPTVFFLR[a,b,c,d,e,f]	EVSVVDILSHASVWLFR[d]	17	0.091
UGT1A4	YLSIPAVFFWR[a,c,d,e,f]	VTLGYTQGFFETEHLLK[d]	16	0.900
UGT1A6	DIVEVLSDR[a,c,d,e,f]	SFLTAPQTEYR[b,d]	15	0.986
		DVDIITLYQK[c]	16	0.979
UGT1A9	AFAHAQWK[c,d,f]	GHEVVVVMPEVSWQLGR	16	0.867
		ESSFDAVFLDPFDNCGLIVAK[b]	17	0.703
UGT2B4	FSPGYAIEK[a,b,c,d,e]	TILDELVQR	16	0.974
		ANVIASALAK[b]	17	0.956
UGT2B7	ADVWLIR[a,b,d,e]	TILDELIQR[b,c,f]	16	0.906
		IEIYPTSLTK[d]	13	0.962
		ANVIASALAQIPQK	15	0.886
UGT2B10	ANVIATALAK[h]	GHEVTVLASSASILFDPNDSSTLK[d,e]	17	0.956
		DTFWLPFSQEQEILWAINDIIR[b]	17	0.321
UGT2B15	FSVGYTFEK[a,d,f]	WIYGVSK[b]	16	0.900
		SVINDPVYK[b,c,d]	16	0.982
UGT2B17	FSVGYTVEK[d,e]	None	ND	ND

[a]Achour et al., 2017.
[b]Achour et al., 2018.
[c]Bhatt et al., 2018.
[d]Fallon et al., 2013.
[e]Khatri et al., 2019.
[f]Sato et al., 2014.
[g]Peptide also present in UGT1A7 sequence.
[h]Peptide also present in UGT2B11 and 2B28 sequences.

activity probes, reflecting the lesser contribution of CYP3A5 to total metabolism.

UGT1A enzymes showed moderate-to-strong correlations of expression and activities (rs = 0.51–0.86; Table 3). Additional drugs known to have high enzyme selectivity were tested for UGT1A1 (dolutegravir and raltegravir), 1A4 (lamotrigine), and 1A9 (mycophenolic acid). The tested drugs showed comparable correlations with expression as the probe substrates, supporting that they are predominantly conjugated by

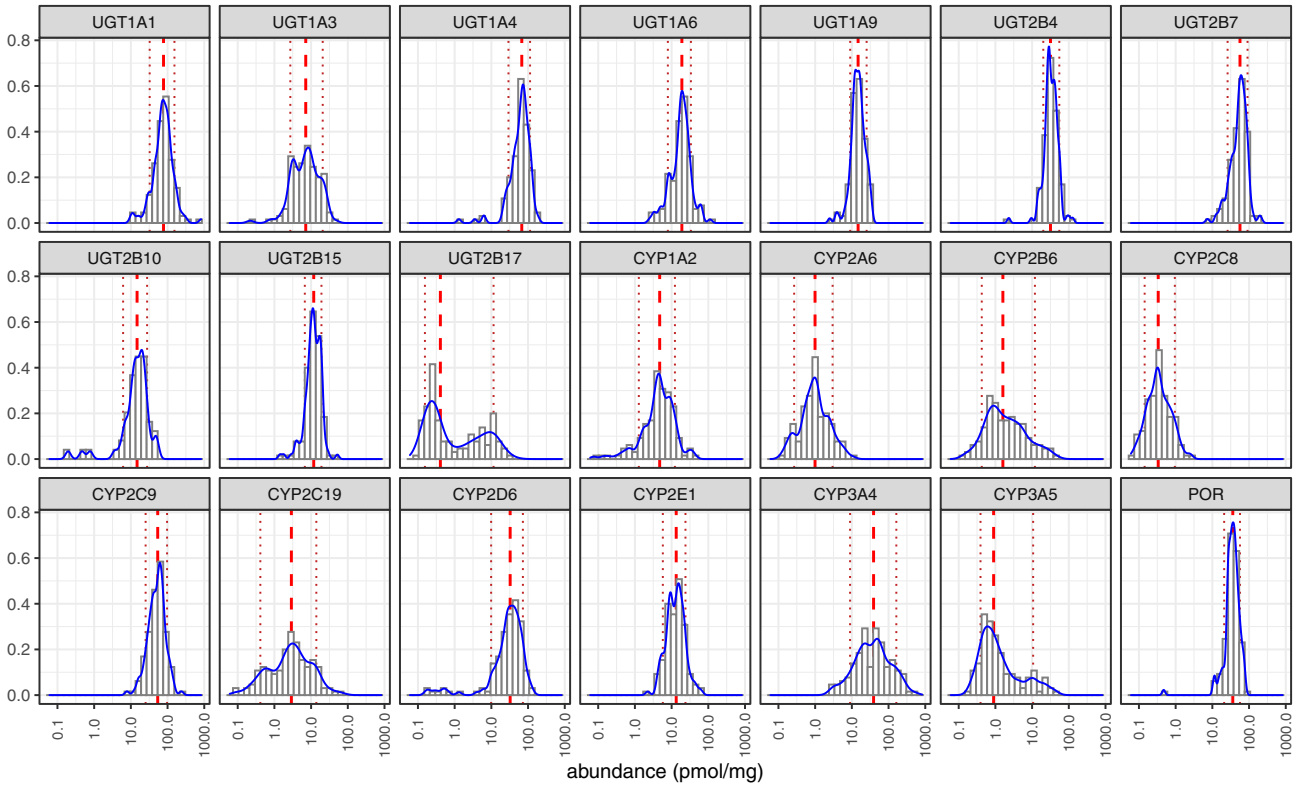

Fig. 1. Frequency distribution of UGT and P450 expression within the set of liver samples under study. Blue solid line shows spline fit for the distribution, red dashed line shows median of results, and dotted red lines show 10% and 90% percentiles of results.
POR, cytochrome P450 reductase.

TABLE 2

UGT expression measured for single-donor and 200-donor pooled human liver microsomes by LC-MS/MS.

For single-donor HLM, 10th, 50th (median), and 90th percentiles, and range are presented to describe the study's population data and mean is presented to compare with the pooled HLM. CV, % for pooled HLM is presented to describe measurement variability and represents n = 4 replicates in one analytical batch.

	Expression (pmol/mg)						
	Single-Donor HLM (n = 130 except for UGT2B10, which was n = 49)				Single-Donor HLM (n = 130)	200-Donor Pooled HLM (n = 4 measurements)	
Enzyme	10th Percentile	Median	90th Percentile	Range (90:10 percentiles)	Mean	Mean	CV (%)
UGT1A1	35.2	80.7	165	4.7	102	68.5	8.63
UGT1A3	2.72	7.64	21.9	8.1	9.76	6.07	5.70
UGT1A4	29.1	67.4	114	3.9	69.2	67.9	7.02
UGT1A6	8.24	19.5	37.2	4.5	23.3	20.2	9.45
UGT1A9	9.22	15.0	26.8	2.9	16.2	15.8	9.71
UGT2B4	22.7	36.1	59.9	2.6	39.8	31.9	3.84
UGT2B7	26.9	61.2	111	4.1	66.7	45.5	10.0
UGT2B10	9.94	23.8	44.7	4.5	27.5	12.3	4.51
UGT2B15	7.41	12.6	29.7	4.0	16.2	11.0	22.1
UGT2B17	0.170	0.455	13.4	79	4.63	2.23	11.4

the respective UGT1A enzymes, with minor contributions by other UGTs (Picard et al., 2005; Rowland et al., 2006; Kassahun et al., 2007; Argikar and Remmel, 2009; Reese et al., 2013; Liu et al., 2019). Correlation of UGT1A9 abundance with mycophenolic acid glucuronidation was reasonable (rs = 0.63), but with propofol, an accepted probe substrate for UGT1A9, the degree of correlation was lower than expected (rs = 0.52).

Weak-to-moderate correlations were observed for UGT2B activities and measured expressions (Table 3). UGT2B4 expression showed some correlation with gemfibrozil glucuronidation, a nonselective substrate (rs = 0.43), and was not improved when a UGT2B7 inhibitor was added (rs = 0.38). Multiple substrates were tested for UGT2B7, and they showed no correlation except zidovudine, which showed a moderate correlation (rs = 0.34). Amitryptyline activities showed moderate correlation with UGT2B10 expression (rs = 0.31), whereas the more selective substrate RO5263397 (Milani et al., 2020) showed higher correlation (rs = 0.53), and (*S*)-oxazepam activities showed low correlation with UGT2B15 expression (rs = 0.28). UGT2B17 abundance showed higher correlation with testosterone glucuronidation (rs = 0.58), potentially benefiting from a wider dynamic range of enzyme expression.

Discussion

Ten major UGT enzymes (as our primary interest) and ten major drug-metabolizing P450s (as comparators) were monitored to test and validate our methodological approaches. P450s were efficiently assessed for peptide release with simple denaturation, alkylation, and tryptic digestion. In contrast, adding detergent (CelLytic M) and increasing trypsin:protein ratios increased recoveries of UGT peptides. This was unsurprising, as UGTs localize to the luminal face of microsomes and are likely to be poorly accessed by trypsin. The linearity of the method was confirmed by selectively combining single-donor HLM samples to span the full range of expressions (Supplemental Fig. 1). This strategy for linearity assessment adds to traditional approaches of standard

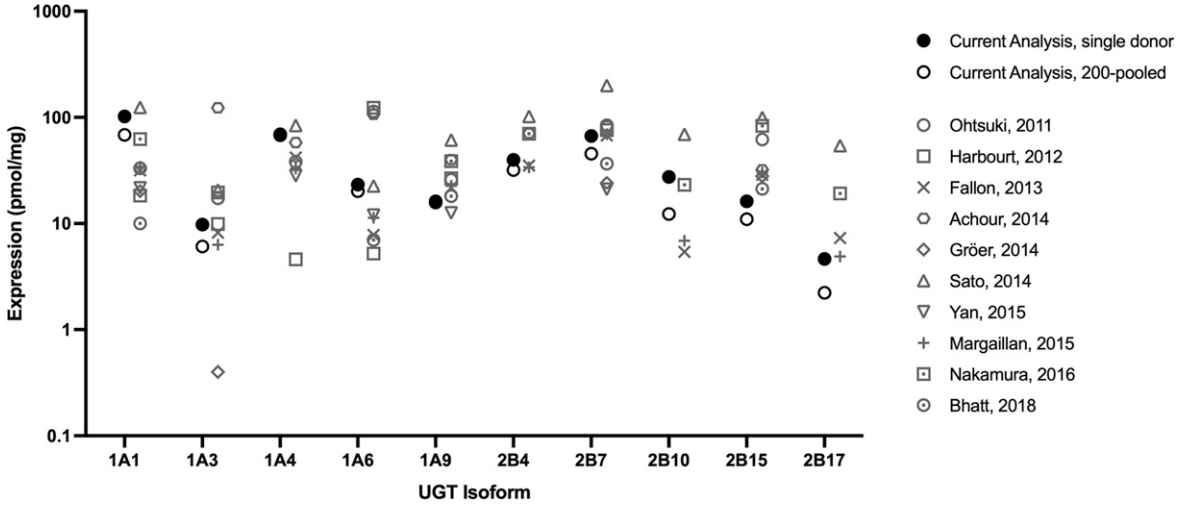

Fig. 2. Mean UGT abundance reported in various UGT proteomics studies. Comparison of hepatic expression levels measured in the current study [mean of single donor, n = 130 (filled circles), and 200-pooled human microsomes (open circles)] with previous reports for UGT enzymes (Ohtsuki et al., 2011; Harbourt et al., 2012; Fallon et al., 2013; Achour et al., 2014b; Gröer et al., 2014; Sato et al., 2014; Margaillan et al., 2015; Yan et al., 2015; Nakamura et al., 2016; Bhatt et al., 2018).

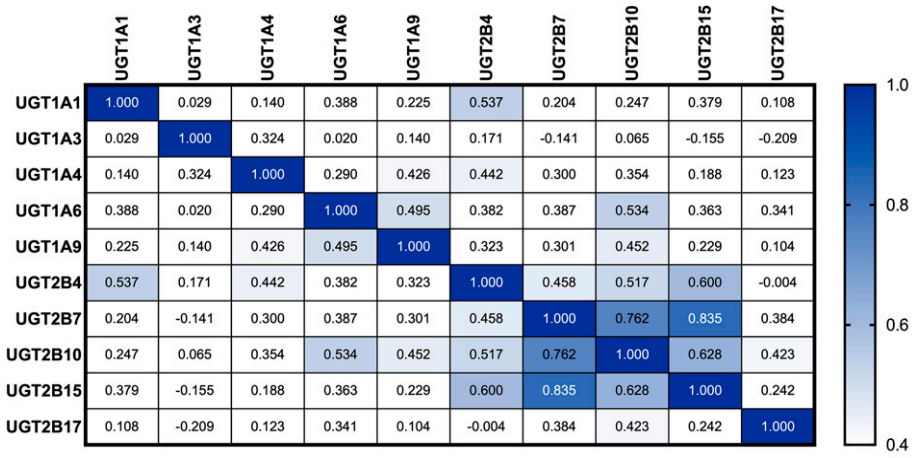

Fig. 3. Correlation matrix of UGT enzymes (expression versus expression) observed with single-donor human liver microsomes. Values are Spearman correlations (rs). Expression data for each enzyme describes 130 single donors except for UGT2B10, which was 49 single donors.

additions of synthetic peptides (non-SIL and SIL) to surrogate blank or matched matrices. This approach is resource-sparing, simultaneously assessed linearity of trypsin digestion and LC-MS/MS measurement, and was deemed appropriate for quantifying interindividual variability for each enzyme.

We monitored multiple peptides for each target protein to indicate the consistency of our proteomics approach. Where two peptides are equally subject to tryptic digestion efficiency and recovery, polymorphic variation, post-translational modification, and stability in analysis, the ratio of peptides arising from the same protein should be fixed, and their abundances should correlate. This occurred for almost all peptide pairs (Table 1), with notable exceptions being UGT1A3 and UGT2B10. For UGT1A3, the peptide EVSVVDILSHASVWLFR showed a small dynamic range, indicating this peptide was not suitable. Fallon et al. (2013) reported lack of sensitivity using this peptide. A more successful approach has been monitoring the peptide YLSIPTVFFLR (Achour et al., 2017, 2018; Khatri et al., 2019). Our analysis using this peptide resulted in highly correlated enzyme concentration with activities measured using chenodeoxycholic acid (rs = 0.85). For UGT2B10, the peptide ANVIATALAK was selected and analyzed using its SIL analog after initial experiments using peptide DTFWLPFSQEQEILWAINDIIR showed its limitations. Some reports describe GHEVTVLASSASILFDPN**D**SSTLK as a preferred peptide for quantification (Fallon et al., 2013; Khatri et al., 2019), although it spans the D67Y polymorphism site. As shown in Fig. 4, these peptides are regionally distinct, so their release with trypsin treatment should not be linked. Unfortunately,

TABLE 3

Correlation of enzyme expression with enzymatic activities measured with probe substrate reactions

Enzyme	Reaction/Substrate	Spearman Correlation (rs)	*n*
UGT1A1	Dolutegravir	0.795	62
	17β-Estradiol (3OH-glucuronidation)	0.782	62
	Raltegravir	0.783	79
UGT1A3	Chenodeoxycholic acid	0.846	62
UGT1A4	Trifluoperazine	0.729	62
	Lamotrigine	0.793	62
UGT1A6	5-Hydroxytryptofol	0.856	62
UGT1A9	Propofol	0.512	62
	Mycophenolic acid	0.587	79
UGT2B4	Gemfibrozil	0.433	62
	Gemfibrozil (with inclusion of UGT2B7 inhibitor)	0.379	62
UGT2B7	Zidovudine	0.344	62
	Ketoprofen	0.172	62
UGT2B10	RO5263397	0.529	32
	Amitriptyline	0.308	32
UGT2B15	(*S*)-Oxazepam	0.283	63
UGT2B17	Testosterone	0.582	62
CYP1A2	Phenacetin *O*-dealkylation	0.839	65
	Ethoxyresorufin *O*-deethylation	0.804	43
CYP2A6	Coumarin 7-hydroxylation	0.864	107
CYP2B6	(S)-Mephenytoin *N*-demethylation	0.696	84
	Bupropion hydroxylation	0.916	20
CYP2C8	Paclitaxel 6α-hydroxylation	0.768	37
	Amodiaquine *N*-dealkylation	0.830	64
CYP2C9	Diclofenac 4'-hydroxylation	0.734	107
CYP2C19	(S)-Mephenytoin 4'-hydroxylation	0.876	99
CYP2D6	Dextromethorphan *O*-demethylation	0.853	107
CYP2E1	Chlorzoxazone 6-hydroxylation	0.758	107
CYP3A4	Testosterone 6β-hydroxylation	0.923	107
	Midazolam 1′-hydroxylation	0.837	63
CYP3A5	Testosterone 6β-hydroxylation	0.426	107
	Midazolam 1′-hydroxylation	0.550	63

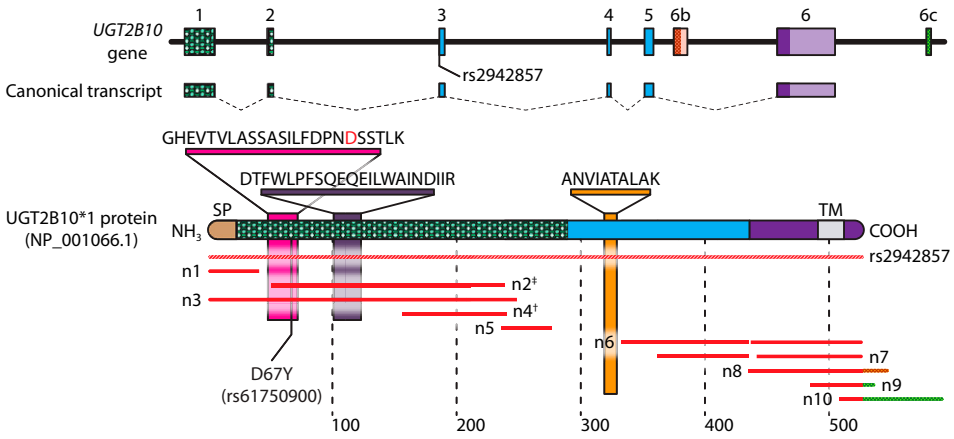

Fig. 4. Diagram of the UGT2B10 amino acid sequence illustrating the locations of the proteomic reporting peptides, amino acid polymorphisms, and key splice variants. Red bars underneath the diagram of the canonical protein indicate regions that would be absent in the proteins encoded by the splice variants identified to date. The intronic SNP rs2942857 is predicted to produce an unstable mRNA that would be degraded before the protein is produced. Splice variants incorporating alternate versions of exon 6 are colored to match the exon map. The signal peptide (SP) is indicated in tan, the substrate binding domain in dotted green, the UDPGA cosubstrate binding domain in cyan, the C-terminal region in purple, and the transmembrane domain (TM) in silver. †Variant n4 corresponds to National Center for Biotechnology Information GenBank isoform 2 (NP_001138239.1). ‡Variant n2 corresponds to National Center for Biotechnology Information GenBank isoform 3 (NP_001277020.1).

ANV … K cannot be regarded as a completely selective peptide for UGT2B10, as this sequence is also present in human UGT2B11 and UGT2B28, which share 90% and 89% amino acid sequence identity, respectively, with UGT2B10 (Ohno and Nakajin, 2011). UGT2B28 has been reported to have little or no hepatic expression and is therefore unlikely to have interfered with UGT2B10 analysis (Nakamura et al., 2008; Ohno and Nakajin, 2011). Some contribution by UGT2B11 to signal in the proteomics measurement is possible, which could reduce the abundance-activity correlation. Anecdotally, the poor metabolizer phenotype donor H0295 (Milani et al., 2020) gave an extremely low but nonzero UGT2B10 abundance signal, which may be indicative of background ANV … K signal coming from other sources in liver microsomes. GHE … K abundance correlated very highly with ANV … K (rs = 0.956), further indicating a relatively low level of signal contamination in the HLM samples assessed.

Assessment of large numbers of individual donor samples often requires batching of samples. We accounted for batch effects by normalizing to a QC sample that was included for each preparation and analysis. Our QC sample was a 200-donor pooled HLM sample (XT-200, Xenotech). A QC normalization approach becomes more valuable if a consensus sample is used across analysts, laboratories, and time, as demonstrated in a meta-analysis of UGT abundance studies using immunoblotting approaches (Liu et al., 2020).

Here, we showed in a large liver panel that population mean expression values vary maximally 2-fold from that of the pooled HLM samples, and the 10th to 90th percentile ranges were 8-fold or less (excepting UGT2B17). In contrast, 10- to 100-fold differences in mean concentrations were found between studies (Fig. 2). Although inherent to interlaboratory variability is the analysis of different liver samples, the current data set indicates that the large range in reported values is methodological (different experimental and analytical protocols) in its origin rather than population variability.

P450 analyses were used to anchor method quality, validate the strategy of correlating enzyme expression with activity, and generate additional data on P450 expression distribution. Strong correlations (rs = 0.6–0.9) were observed, confirming the simple more enzyme equals more activity assumption and validating our methodological approach. For UGTs, a more complex picture emerged. Strong correlations were observed for UGT1A1, 1A3, 1A4, and 1A6 (rs $>$ 0.75), but there was less association of measured expression with activities for the other studied UGTs. One limiting factor for correlation is the dynamic range of the measured UGT concentrations. The 10th to 90th percentile ranges were relatively small, potentially limiting the obtainable correlation coefficients when taking into account inaccuracies in enzyme activity and enzyme concentration measurements.

We observed little correlation of enzymatic activities with expression for UGT2B7, UGT2B10, and UGT2B15 despite using validated substrates for these enzymes. The low correlations for UGT2B7 were surprising in light of previous proteomics-activity correlation reports of rs = 0.82 (Margaillan et al., 2015) or rs = 0.79 (Achour et al., 2017) and rs = 0.52 (Achour et al., 2018), where zidovudine was used as probe substrate, as well as ketoprofen and zidovudine activities being highly correlated in our previous work (Badée et al., 2019b). Although additional UGTs other than UGT2B15 may contribute to (*S*)-oxazepam glucuronidation and account for lower expression-activity correlation (rs = 0.28), glucuronidation of RO5263397 at the concentrations tested is expected to be almost exclusively UGT2B10-mediated, and higher expression-activity correlation than observed (rs = 0.53) was expected. Numerous studies have explored the potential for multiple UGTs to contribute to glucuronidation of probe substrates, dependent upon substrate concentration and reaction conditions (Lv et al., 2019; Miners et al., 2021). We noted that the highest intercorrelation in expression of UGTs across the single-donor liver samples existed for UGT2B7, 2B10, and 2B15 (Fig. 3, rs ranging 0.63-0.84).

Proteomics approaches may not differentiate functional, incompletely expressed, and nonfunctional proteins resulting from genetic variation. The detection or nondetection of some variants could disrupt activity-abundance correlations. This has highest potential to impact measurements of UGT2B isoforms. Unlike the UGT1A family, the UGT2B genes are produced from distinct gene loci with no shared exons. Exons 1 and 2 of each UGT2B gene code approximately the first 290 amino acids roughly corresponding to the substrate selective N-terminal end, with exons 3–5 mostly coding the more conserved sugar binding domain (Hu et al., 2019). The UGT2B genes encode between 7 and 44 alternatively spliced transcripts depending on the gene and varying based on tissue and disease state (Rouleau et al., 2016; Tourancheau et

al., 2016). High levels of alternatively spliced transcripts for UGT2Bs (UGT2B4: 16%, UGT2B7: 8%, UGT2B10: 62%, UGT2B15: 6%, UGT2B17: 37%) have been found in the liver (Tourancheau et al., 2018).

UGT2B10 is a good example of this genetic variation and its potential impact in proteomics approaches (Fig. 4). Including the canonical sequence, there are eleven UGT2B10 splice variants (Rouleau et al., 2016; Tourancheau et al., 2016, 2018), all of which would be captured by at least one of the reporter peptides (Fig. 4). There are also over 5000 SNPs present in the reference sequence, 638 of which result in protein alterations, including 78 located in the regions detected by the peptides. Peptide ANV … K has the fewest protein-altering SNPs (14), whereas DTF … R (42 SNPs) and GHE … K (22 SNPs) have more protein-altering SNPs at their locations. As ANV … K is closest to the C-terminal end of the protein, it is less likely to be affected by frameshift or protein-truncating mutations that result in nonfunctional proteins. Two UGT2B10 SNPs have been explicitly associated with a clinically relevant phenotype. The UGT2B10*2 allele (rs61750900, Asp67Tyr), present in ∼11% of Caucasians (which constitute the majority of donor samples in this study) and ∼5% of African Americans, is located within the region captured by the GHE … K peptide, and results in functional impairment (Chen et al., 2008; Berg et al., 2010; Bloom et al., 2013; Sipe et al., 2020). A second polymorphism (rs2942857) located at the splice-acceptor site between intron 2 and exon 3, present in ∼0.4% of Caucasians and ∼36% of African Americans, is believed to produce an unstable mRNA that fails to produce a viable protein. Individuals homozygous for this SNP present a UGT2B10-null phenotype and exhibit essentially no UGT2B10-related drug clearance (Fowler et al., 2015; Labriet et al., 2018; Sipe et al., 2020).

Additional alignments of UGT2B sequences and exon maps indicate that most polymorphisms would be captured by our reporter peptides. UGT2B7 has the largest number of splice variants of any UGT at 44, with only the canonical product being shown to have any functional activity to date, despite at least seven different proteins being produced from the first 22 splice variants alone (Ménard et al., 2009; Tourancheau et al., 2018). The peptides would capture 36 of the possible variants. The nine UGT2B15, and at least eight of the 10 UGT2B17 splice variants, would also be captured by at least one of the peptides for their respective products. Exceptions are polymorphisms not producing protein from any of the canonical exons, such as the UGT2B17*2 allele, common in Asian populations (Jakobsson et al., 2006). We recognize the potential for future proteomics studies to capture nonsynonymous or splice variant distribution, in addition to expression distribution, with strategically selected peptides.

In this study, we applied LC-MS/MS methodologies to quantify hepatic UGTs. With the exception of UGT2B17, 10th to 90th percentile ranges of UGT expression were between 3- and 8-fold and smaller than indicated by interlaboratory ranges. Combined proteomics and activity measurements provided new insights and revealed complexities of UGT enzymology and methodologies. These findings will be important for accurately translating UGT characterization data to estimates of drug clearance, population variability, and enzyme ontogeny and should be borne in mind by constructors of PBPK models for UGT substrates.

Acknowledgments

The authors thank Dr. Brian Ogilvie, Vice President of Scientific Consulting at Sekisui XenoTech, for granting permission to use P450 enzymatic activities from product data sheets for correlation analysis.

Authorship Contributions

Participated in research design: Takahashi, Fowler.

Conducted experiments: Takahashi.

Contributed new reagents or analytic tools: Forrest.

Performed data analysis: Takahashi, Forrest, Badee, Qiu, Schmidt, Collier, Parrott, Fowler.

Contributed to the writing of the manuscript: Takahashi, Smith, Badee, Schmidt, Collier, Parrott, Fowler.

References

Achour B, Barber J, and Rostami-Hodjegan A (2014a) Expression of hepatic drug-metabolizing cytochrome p450 enzymes and their intercorrelations: a meta-analysis. *Drug Metab Dispos* **42**:1349–1356.

Achour B, Dantonio A, Niosi M, Novak JJ, Al-Majdoub ZM, Goosen TC, Rostami-Hodjegan A, and Barber J (2018) Data generated by quantitative liquid chromatography-mass spectrometry proteomics are only the start and not the endpoint: Optimization of quantitative concatemer-based measurement of hepatic uridine-5′-diphosphate-glucuronosyltransferase enzymes with reference to catalytic activity. *Drug Metab Dispos* **46**:805–812.

Achour B, Dantonio A, Niosi M, Novak JJ, Fallon JK, Barber J, Smith PC, Rostami-Hodjegan A, and Goosen TC (2017) Quantitative characterization of major hepatic UDP-glucuronosyltransferase enzymes in human liver microsomes: Comparison of two proteomic methods and correlation with catalytic activity. *Drug Metab Dispos* **45**:1102–1112.

Achour B, Russell MR, Barber J, and Rostami-Hodjegan A (2014b) Simultaneous quantification of the abundance of several cytochrome P450 and uridine 5′-diphospho-glucuronosyltransferase enzymes in human liver microsomes using multiplexed targeted proteomics. *Drug Metab Dispos* **42**:500–510.

Argikar UA, Potter PM, Hutzler JM, and Marathe PH (2016) Challenges and opportunities with non-P450 enzymes aldehyde oxidase, carboxylesterase, and UDP-glucuronosyltransferase: Focus on reaction phenotyping and prediction of human clearance. *AAPS J* **18**:1391–1405.

Argikar UA and Remmel RP (2009) Variation in glucuronidation of lamotrigine in human liver microsomes. *Xenobiotica* **39**:355–363.

Badée J, Fowler S, de Wildt SN, Collier AC, Schmidt S, and Parrott N (2019a) The ontogeny of UDP-glucuronosyltransferase enzymes, recommendations for future profiling studies and application through physiologically based pharmacokinetic modelling. *Clin Pharmacokinet* **58**:189–211.

Badée J, Qiu N, Collier AC, Takahashi RH, Forrest WF, Parrott N, Schmidt S, and Fowler S (2019b) Characterization of the ontogeny of hepatic UDP-glucuronosyltransferase enzymes based on glucuronidation activity measured in human liver microsomes. *J Clin Pharmacol* **59** (Suppl 1):S42–S55.

Badée J, Qiu N, Parrott N, Collier AC, Schmidt S, and Fowler S (2019c) Optimization of experimental conditions of automated glucuronidation assays in human liver microsomes using a cocktail approach and ultra-high performance liquid chromatography-tandem mass spectrometry. *Drug Metab Dispos* **47**:124–134.

Basit A, Neradugomma NK, Wolford C, Fan PW, Murray B, Takahashi RH, Khojasteh SC, Smith BJ, Heyward S, Totah RA, et al. (2020) Characterization of differential tissue abundance of major non-P450 enzymes in human. *Mol Pharm* **17**:4114–4124.

Berg JZ, Mason J, Boettcher AJ, Hatsukami DK, and Murphy SE (2010) Nicotine metabolism in African Americans and European Americans: variation in glucuronidation by ethnicity and UGT2B10 haplotype. *J Pharmacol Exp Ther* **332**:202–209.

Bhatt DK, Basit A, Zhang H, Gaedigk A, Lee SB, Claw KG, Mehrotra A, Chaudhry AS, Pearce RE, Gaedigk R, et al. (2018) Hepatic abundance and activity of androgen- and drug-metabolizing enzyme UGT2B17 are associated with genotype, age, and sex. *Drug Metab Dispos* **46**:888–896.

Bhatt DK, Mehrotra A, Gaedigk A, Chapa R, Basit A, Zhang H, Choudhari P, Boberg M, Pearce RE, Gaedigk R, et al. (2019) Age- and genotype-dependent variability in the protein abundance and activity of six major uridine diphosphate-glucuronosyltransferases in human liver. *Clin Pharmacol Ther* **105**:131–141.

Bhatt DK and Prasad B (2018) Critical issues and optimized practices in quantification of protein abundance level to determine interindividual variability in DMET proteins by LC-MS/MS proteomics. *Clin Pharmacol Ther* **103**:619–630.

Bloom AJ, von Weymarn LB, Martinez M, Bierut LJ, Goate A, and Murphy SE (2013) The contribution of common UGT2B10 and CYP2A6 alleles to variation in nicotine glucuronidation among European Americans. *Pharmacogenet Genomics* **23**:706–716.

Cerny MA (2016) Prevalence of non-cytochrome P450-mediated metabolism in food and drug administration-approved oral and intravenous drugs: 2006-2015. *Drug Metab Dispos* **44**:1246–1252.

Chen G, Dellinger RW, Gallagher CJ, Sun D, and Lazarus P (2008) Identification of a prevalent functional missense polymorphism in the UGT2B10 gene and its association with UGT2B10 inactivation against tobacco-specific nitrosamines. *Pharmacogenet Genomics* **18**:181–191.

Docci L, Umehara K, Krähenbühl S, Fowler S, and Parrott N (2020) Construction and verification of physiologically based pharmacokinetic models for four drugs majorly cleared by glucuronidation: Lorazepam, oxazepam, naloxone, and zidovudine. *AAPS J* **22**:128.

Fallon JK, Neubert H, Hyland R, Goosen TC, and Smith PC (2013) Targeted quantitative proteomics for the analysis of 14 UGT1As and -2Bs in human liver using NanoUPLC-MS/MS with selected reaction monitoring. *J Proteome Res* **12**:4402–4413.

Fowler S, Kletzl H, Finel M, Manevski N, Schmid P, Tuerck D, Norcross RD, Hoener MC, Spleiss O, and Iglesias VA (2015) A UGT2B10 splicing polymorphism common in african populations may greatly increase drug exposure. *J Pharmacol Exp Ther* **352**:358–367.

Gröer C, Busch D, Patrzyk M, Beyer K, Busemann A, Heidecke CD, Drozdzik M, Siegmund W, and Oswald S (2014) Absolute protein quantification of clinically relevant cytochrome P450 enzymes and UDP-glucuronosyltransferases by mass spectrometry-based targeted proteomics. *J Pharm Biomed Anal* **100**:393–401.

Harbourt DE, Fallon JK, Ito S, Baba T, Ritter JK, Glish GL, and Smith PC (2012) Quantification of human uridine-diphosphate glucuronosyl transferase 1A isoforms in liver, intestine, and kidney using nanobore liquid chromatography-tandem mass spectrometry. *Anal Chem* **84**:98–105.

Howgate EM, Rowland Yeo K, Proctor NJ, Tucker GT, and Rostami-Hodjegan A (2006) Prediction of in vivo drug clearance from in vitro data. I: impact of inter-individual variability. *Xenobiotica* **36**:473–497.

Hu DG, Hulin JU, Nair PC, Haines AZ, McKinnon RA, Mackenzie PI, and Meech R (2019) The UGTome: The expanding diversity of UDP glycosyltransferases and its impact on small molecule metabolism. *Pharmacol Ther* **204**:107414.

Jakobsson J, Ekström L, Inotsume N, Garle M, Lorentzon M, Ohlsson C, Roh HK, Carlström K, and Rane A (2006) Large differences in testosterone excretion in Korean and Swedish men are strongly associated with a UDP-glucuronosyl transferase 2B17 polymorphism. *J Clin Endocrinol Metab* **91**:687–693.

Jones HM, Chen Y, Gibson C, Heimbach T, Parrott N, Peters SA, Snoeys J, Upreti VV, Zheng M, and Hall SD (2015) Physiologically based pharmacokinetic modeling in drug discovery and development: a pharmaceutical industry perspective. *Clin Pharmacol Ther* **97**:247–262.

Kassahun K, McIntosh I, Cui D, Hreniuk D, Merschman S, Lasseter K, Azrolan N, Iwamoto M, Wagner JA, and Wenning LA (2007) Metabolism and disposition in humans of raltegravir (MK-0518), an anti-AIDS drug targeting the human immunodeficiency virus 1 integrase enzyme. *Drug Metab Dispos* **35**:1657–1663.

Khatri R, Fallon JK, Rementer RJB, Kulick NT, Lee CR, and Smith PC (2019) Targeted quantitative proteomic analysis of drug metabolizing enzymes and transporters by nano LC-MS/MS in the sandwich cultured human hepatocyte model. *J Pharmacol Toxicol Methods* **98**:106590.

Labriet A, Allain EP, Rouleau M, Audet-Delage Y, Villeneuve L, and Guillemette C (2018) Post-transcriptional regulation of UGT2B10 hepatic expression and activity by alternative splicing. *Drug Metab Dispos* **46**:514–524.

Liu SN, Lu JBL, Watson CJW, Lazarus P, Desta Z, and Gufford BT (2019) Mechanistic assessment of extrahepatic contributions to glucuronidation of integrase strand transfer inhibitors. *Drug Metab Dispos* **47**:535–544.

Liu Y, Badée J, Takahashi RH, Schmidt S, Parrott N, Fowler S, Mackenzie PI, Coughtrie MWH, and Collier AC (2020) Coexpression of human hepatic uridine diphosphate glucuronosyltransferase proteins: Implications for ontogenetic mechanisms and isoform coregulation. *J Clin Pharmacol* **60**:722–733.

Lv X, Zhang J-B, Hou J, Dou T-Y, Ge G-B, Hu W-Z, and Yang L (2019) Chemical probes for human UDP-glucuronosyltransferases: a comprehensive review. *Biotechnol J* **14**:e1800002.

MacLean B, Tomazela DM, Shulman N, Chambers M, Finney GL, Frewen B, Kern R, Tabb DL, Liebler DC, and MacCoss MJ (2010) Skyline: an open source document editor for creating and analyzing targeted proteomics experiments. *Bioinformatics* **26**:966–968.

Margaillan G, Rouleau M, Klein K, Fallon JK, Caron P, Villeneuve L, Smith PC, Zanger UM, and Guillemette C (2015) Multiplexed targeted quantitative proteomics predicts hepatic glucuronidation potential. *Drug Metab Dispos* **43**:1331–1335.

Ménard V, Girard H, Harvey M, Pérusse L, and Guillemette C (2009) Analysis of inherited genetic variations at the UGT1 locus in the French-Canadian population. *Hum Mutat* **30**:677–687.

Milani N, Qiu N, Molitor B, Badée J, Cruciani G, and Fowler S (2020) Use of phenotypically poor metabolizer individual donor human liver microsomes to identify selective substrates of UGT2B10. *Drug Metab Dispos* **48**:176–186.

Miners JO, Rowland A, Novak JJ, Lapham K, and Goosen TC (2021) Evidence-based strategies for the characterisation of human drug and chemical glucuronidation in vitro and UDP-glucuronosyltransferase reaction phenotyping. *Pharmacol Ther* **218**:107689.

Nakamura A, Nakajima M, Yamanaka H, Fujiwara R, and Yokoi T (2008) Expression of UGT1A and UGT2B mRNA in human normal tissues and various cell lines. *Drug Metab Dispos* **36**:1461–1464.

Nakamura K, Hirayama-Kurogi M, Ito S, Kuno T, Yoneyama T, Obuchi W, Terasaki T, and Ohtsuki S (2016) Large-scale multiplex absolute protein quantification of drug-metabolizing enzymes and transporters in human intestine, liver, and kidney microsomes by SWATH-MS: Comparison with MRM/SRM and HR-MRM/PRM. *Proteomics* **16**:2106–2117.

Ohno S and Nakajin S (2011) Quantitative analysis of UGT2B28 mRNA expression by real-time RT-PCR and application to human tissue distribution study. *Drug Metab Lett* **5**:202–208.

Ohtsuki S, Uchida Y, Kubo Y, and Terasaki T (2011) Quantitative targeted absolute proteomics-based ADME research as a new path to drug discovery and development: methodology, advantages, strategy, and prospects. *J Pharm Sci* **100**:3547–3559.

Picard N, Ratanasavanh D, Prémaud A, Le Meur Y, and Marquet P (2005) Identification of the UDP-glucuronosyltransferase isoforms involved in mycophenolic acid phase II metabolism. *Drug Metab Dispos* **33**:139–146.

Prasad B, Achour B, Artursson P, Hop CECA, Lai Y, Smith PC, Barber J, Wisniewski JR, Spellman D, Uchida Y, et al. (2019) Toward a consensus on applying quantitative liquid chromatography-tandem mass spectrometry proteomics in translational pharmacology research: A white paper. *Clin Pharmacol Ther* **106**:525–543.

Prasad B, Vrana M, Mehrotra A, Johnson K, and Bhatt DK (2017) The promises of quantitative proteomics in precision medicine. *J Pharm Sci* **106**:738–744.

Proctor NJ, Tucker GT, and Rostami-Hodjegan A (2004) Predicting drug clearance from recombinantly expressed P450s: intersystem extrapolation factors. *Xenobiotica* **34**:151–178.

Reese MJ, Savina PM, Generaux GT, Tracey H, Humphreys JE, Kanaoka E, Webster LO, Harmon KA, Clarke JD, and Polli JW (2013) In vitro investigations into the roles of drug transporters and metabolizing enzymes in the disposition and drug interactions of dolutegravir, a HIV integrase inhibitor. *Drug Metab Dispos* **41**:353–361.

Rouleau M, Tourancheau A, Girard-Bock C, Villeneuve L, Vaucher J, Duperré AM, Audet-Delage Y, Gilbert I, Popa I, Droit A, et al. (2016) Divergent expression and metabolic functions of human glucuronosyltransferases through alternative splicing. *Cell Rep* **17**:114–124.

Rowland A, Elliot DJ, Williams JA, Mackenzie PI, Dickinson RG, and Miners JO (2006) In vitro characterization of lamotrigine N2-glucuronidation and the lamotrigine-valproic acid interaction. *Drug Metab Dispos* **34**:1055–1062.

Rowland M, Peck C, and Tucker G (2011) Physiologically-based pharmacokinetics in drug development and regulatory science. *Annu Rev Pharmacol Toxicol* **51**:45–73.

Sato Y, Nagata M, Tetsuka K, Tamura K, Miyashita A, Kawamura A, and Usui T (2014) Optimized methods for targeted peptide-based quantification of human uridine 5′-diphosphate-glucuronosyltransferases in biological specimens using liquid chromatography-tandem mass spectrometry. *Drug Metab Dispos* **42**:885–889.

Sipe CJ, Koopmeiners JS, Donny EC, Hatsukami DK, and Murphy SE (2020) *UGT2B10* genotype influences serum cotinine levels and is a primary determinant of higher cotinine in African American smokers. *Cancer Epidemiol Biomarkers Prev* **29**:1673–1678.

Tourancheau A, Margaillan G, Rouleau M, Gilbert I, Villeneuve L, Lévesque E, Droit A, and Guillemette C (2016) Unravelling the transcriptomic landscape of the major phase II UDP-glucuronosyltransferase drug metabolizing pathway using targeted RNA sequencing. *Pharmacogenomics J* **16**:60–70.

Tourancheau A, Rouleau M, Guauque-Olarte S, Villeneuve L, Gilbert I, Droit A, and Guillemette C (2018) Quantitative profiling of the UGT transcriptome in human drug-metabolizing tissues. *Pharmacogenomics J* **18**:251–261.

Tseng E, Walsky RL, Luzietti Jr RA, Harris JJ, Kosa RE, Goosen TC, Zientek MA, and Obach RS (2014) Relative contributions of cytochrome CYP3A4 versus CYP3A5 for CYP3A-cleared drugs assessed in vitro using a CYP3A4-selective inactivator (CYP3cide). *Drug Metab Dispos* **42**:1163–1173.

Wang YH, Trucksis M, McElwee JJ, Wong PH, Maciolek C, Thompson CD, Prueksaritanont T, Garrett GC, Declercq R, Vets E, et al. (2012) UGT2B17 genetic polymorphisms dramatically affect the pharmacokinetics of MK-7246 in healthy subjects in a first-in-human study. *Clin Pharmacol Ther* **92**:96–102.

Wegler C, Gaugaz FZ, Andersson TB, Wiśniewski JR, Busch D, Gröer C, Oswald S, Norén A, Weiss F, Hammer HS, et al. (2017) Variability in mass spectrometry-based quantification of clinically relevant drug transporters and drug metabolizing enzymes. *Mol Pharm* **14**:3142–3151.

Williams JA, Hyland R, Jones BC, Smith DA, Hurst S, Goosen TC, Peterkin V, Koup JR, and Ball SE (2004) Drug-drug interactions for UDP-glucuronosyltransferase substrates: a pharmacokinetic explanation for typically observed low exposure (AUCi/AUC) ratios. *Drug Metab Dispos* **32**:1201–1208.

Williams JA, Ring BJ, Cantrell VE, Jones DR, Eckstein J, Ruterbories K, Hamman MA, Hall SD, and Wrighton SA (2002) Comparative metabolic capabilities of CYP3A4, CYP3A5, and CYP3A7. *Drug Metab Dispos* **30**:883–891.

Yan T, Gao S, Peng X, Shi J, Xie C, Li Q, Lu L, Wang Y, Zhou F, Liu Z, et al. (2015) Significantly decreased and more variable expression of major P450s and UGTs in liver microsomes prepared from HBV-positive human hepatocellular carcinoma and matched pericarcinomatous tissues determined using an isotope label-free UPLC-MS/MS method. *Pharm Res* **32**:1141–1157.

Address correspondence to: Stephen Fowler, Pharmaceutical Research and Early Development, Roche Innovation Centre Basel, F. Hoffmann-La Roche Ltd, Grenzacherstrasse 124, Basel, CH4070, Switzerland. E-mail: stephen.fowler@roche.com

Supplemental Materials for article DMD-AR-2021-000474:

Characterization of Hepatic UDP-Glucuronosyl Transferase Enzyme Abundance – Activity Correlations and Population Variability using a Proteomics Approach and Comparison with Cytochrome P450 Enzymes

Ryan H. Takahashi, William F. Forrest, Alexander Smith, Justine Badee, NaHong Qiu, Stephan Schmidt, Abby C. Collier, Neil Parrott, Stephen Fowler

Department of Drug Metabolism and Pharmacokinetics (R.H.T.) and Department of OMNI Bioinformatics (W.F.F.), Genentech, Inc., South San Francisco, USA;

Department of Pharmaceutics, Center for Pharmacometrics and Systems Pharmacology (J.B., S.S.), University of Florida at Lake Nona, Orlando, Florida, USA.;

Pharmaceutical Research and Early Development, Roche Innovation Centre Basel, F. Hoffmann-La Roche Ltd. (N.Q., N.P., S.F.), Grenzacherstrasse 124, Basel, Switzerland;

Faculty of Pharmaceutical Sciences, The University of British Columbia (A.S., A.C.C.), Vancouver, BC, Canada.

Corresponding author:

Stephen Fowler, Pharmaceutical Research and Early Development, Roche Innovation Centre Basel, F. Hoffmann-La Roche Ltd, Grenzacherstrasse 124, Basel, CH4070, Switzerland. Phone +41 61 688 5105, email stephen.fowler@roche.com

Footnotes
Current affiliation for R.H.T. is Denali Therapeutics, South San Francisco, CA. Current affiliation for J.B. is Department of PK Sciences, Novartis Institutes for BioMedical Research, Basel, Switzerland.

Supplemental Table 1. Signature Tryptic Peptides Monitored for the Major Human Hepatic CYPs and UGTs and their Respective SRM Information

Protein	Peptide*	Retention time (min)	Q1 (++/+++)	Q3** (+)
CYP				
1A2	IGSTPVLVLS**R**	23.0	571.4 / 576.4++	971.6 / 981.6 (y9) 783.5 / 793.5 (y7) 587.4 / 597.4 (y5)
2A6	GYGVVFSNGE**R**	14.6	592.8 / 597.8++	808.4 / 818.4 (y7) 709.3 / 719.3 (y6) 562.3 / 572.3 (y5)
2B6	TEAFIPFSLG**K**	35.0	605.3 / 609.3++	979.6 / 987.6 (y9) 908.5 / 916.5 (y8) 648.4 / 656.4 (y6)
2C8	GLGIISSNG**K**	8.8	473.3 / 477.3++	775.4 / 783.4 (y8) 605.3 / 613.3 (y6) 492.2 / 500.3 (y5)
2C9	GIFPLAE**R**	22.3	451.8 / 456.8++	732.4 / 742.4 (y6) 585.3 / 595.3 (y5) 488.3 / 498.3 (y4)
2C19	GHFPLAE**R**	5.4	463.7 / 468.7++	732.4 / 742.4 (y6) 585.3 / 595.3 (y5) 488.3 / 498.3 (y4)
2D6	DIEVQGF**R**	15.2	482.2 / 487.3++	735.4 / 745.4 (y6) 606.3 / 616.3 (y5) 507.3 / 517.3 (y4)
2E1	GIIFNNGPTW**K**	26.7	623.8 / 627.8++	963.5 / 971.5 (y8) 816.4 / 824.4 (y7) 702.4 / 710.4 (y6)
3A4	EVTNFL**R**	12.3	439.7 / 444.7++	650.4 / 660.4 (y5) 549.3 / 559.3 (y4) 435.3 / 445.3 (y3)
3A5	DTINFLS**K**	18.4	469.3 / 473.3++	721.4 / 729.4 (y6) 608.3 / 616.4 (y5) 494.3 / 502.3 (y4)
POR	FAVFGLGN**K**	25.5	476.8 / 480.8++	734.4 / 742.4 (y7) 635.4 / 643.4 (y6) 488.3 / 496.3 (y5)
UGT				
1A1	DGAFYTL**K**	15.3	457.7 / 461.7++	742.4 / 750.4+ (y6) 524.3 / 532.3+ (y4) 361.2 / 369.3+ (y3)
1A3	YLSIPTVFFL**R**	40.6	678.4 / 683.4++	1079.6 / 1089.6+ (y9) 992.6 / 1002.6+ (y8) 879.5 / 889.5+ (y7)
1A4	YLSIPAVFFW**R**	42.0	699.9 / 704.9++	1122.7 / 1132.6+ (y9) 1035.6 / 1045.6+ (y8) 922.5 / 932.5+ (y7)

Protein	Peptide*	Retention time (min)	Q1 (++/+++)	Q3** (+)
1A6	DIVEVLSD**R**	24.4	523.3 / 528.3++	817.4 / 827.4 + (y7) 718.4 / 728.4 + (y6) 589.3 / 599.3+ (y5)*
1A9	AFAHAQW**K**	3.6	479.7 / 483.8	740.4 / 748.4+ (y6) 669.3 / 677.4+ (y5) 532.3 / 540.3+ (y4)
2B4	FSPGYAIE**K**	12.6	506.3 / 510.3++	864.4 / 872.5+ (y8) 777.4 / 785.4+ (y7) 680.4 / 688.4+ (y6)
2B7	ADVWLI**R**	23.1	436.8 / 441.8++	686.4 / 696.4+ (y5) 587.4 / 597.4+ (y4) 401.3 / 411.3+ (y3)
2B10	DTFWLPFSQEQEILWAIND II**R**	45.2	912.1 / 915.5+++	1000.6 / 1010.6+ (y8) 814.5 / 824.5+ (y7) 630.4 / 640.4+ (y6)
2B15	FSVGYTFE**K**	22.0	539.3 / 543.3++	930.5 / 938.5+ (y8) 843.4 / 851.4+ (y7) 744.4 / 752.4+ (y6)
2B17	FSVGYTVE**K**	14.6	515.3 / 519.3++	795.4 / 803.4+ (y7) 696.4 / 704.4+ (y6) 375.2 / 383.2+ (y3)

* For stable isotope labeled peptides, the C-terminal lysine or arginine was labeled with ^{13}C and ^{15}N labeled atoms for mass shifts of +8 and +10, respectively.
** Three Q3 ions were monitored for each Q1 ion.

Supplemental Table 2. Linearity of Expression analysis based on mixed HLM experiments

Protein	Nominal Expression (pmol/mg)			Coefficient of Determination (r^2)
	Min	Max	Median	
UGT1A1	11.7	266	117	0.910
UGT1A4	3.50	189	82.8	0.955
UGT2B7	7.35	97.8	45.9	0.879
UGT2B15	1.39	29.6	12.5	0.934
CYP1A2	0.0500	40.8	7.05	0.955
CYP2B6	0.105	46.8	9.75	0.926
CYP2C9	7.83	150	64.8	0.903
CYP2D6	0.165	122	26.6	0.808
CYP3A4	2.51	536	120	0.803

Supplemental Table 3: Correlation of CYP and POR Peptide Concentration in HLM Samples

Protein Target	Quantifier Peptide	Qualifier Peptide(s)	Correlation	
			Sample n	Spearman r
CYP1A2	IGSTPVLVLSR	YGDVLQIR	16	0.994
		YLPNPALQR	16	0.994
		ASGNLIPQEK	16	0.979
CYP2A6	GYGVVFSNGER	GTGGANIDPTFFLSR	17	0.846
		DFIDSFLIR	17	0.919
		SDAFVPFSIGK	17	0.838
CYP2B6	TEAFIPFSLGK	NLQEINAYIGHSVEK	16	0.832
		ETLDPSAPK	16	0.959
CYP2C8	GLGIISSNGK	EALIDNGEEFSGR	16	0.556
		VQEEIDHVIGR	17	0.895
CYP2C9	GIFPLAER	SHMPYTDAVVHEVQR	15	0.893
CYP2C19	GHFPLAER	IYGPVFTLYFGLER	16	0.924
CYP2D6	DIEVQGFR	LLDLAQEGLK	16	0.968
		VQQEIDDVIGQVR	17	0.924
		GTTLITNLSSVLK	17	0.927
CYP2E1	GIIFNNGPTWK	FGPVFTLYVGSQR	16	0.800
		FITLVPSNLPHEATR	17	0.900
		GTVVVPTLDSVLYDNQEFPDPEK	17	0.735
CYP3A4	EVTNFLR	LQEEIDAVLPNK	13	0.995
		LSLGGLLQPEKPVVLK	15	0.989
CYP3A5	DTINFLSK	LGIPGPTPLPLLGNVLSYR	17	0.841
		DSIDPYIYTPFGTGPR	17	0.885
POR	FAVFGLGNK	LEQLGAQR	15	0.871
		TNVLYELAQYASEPSEQELLR	15	0.889
		YYSIASSSK	15	0.843

Supplemental Figure 1: Linearity plots generated with purposely mixed HLM lots

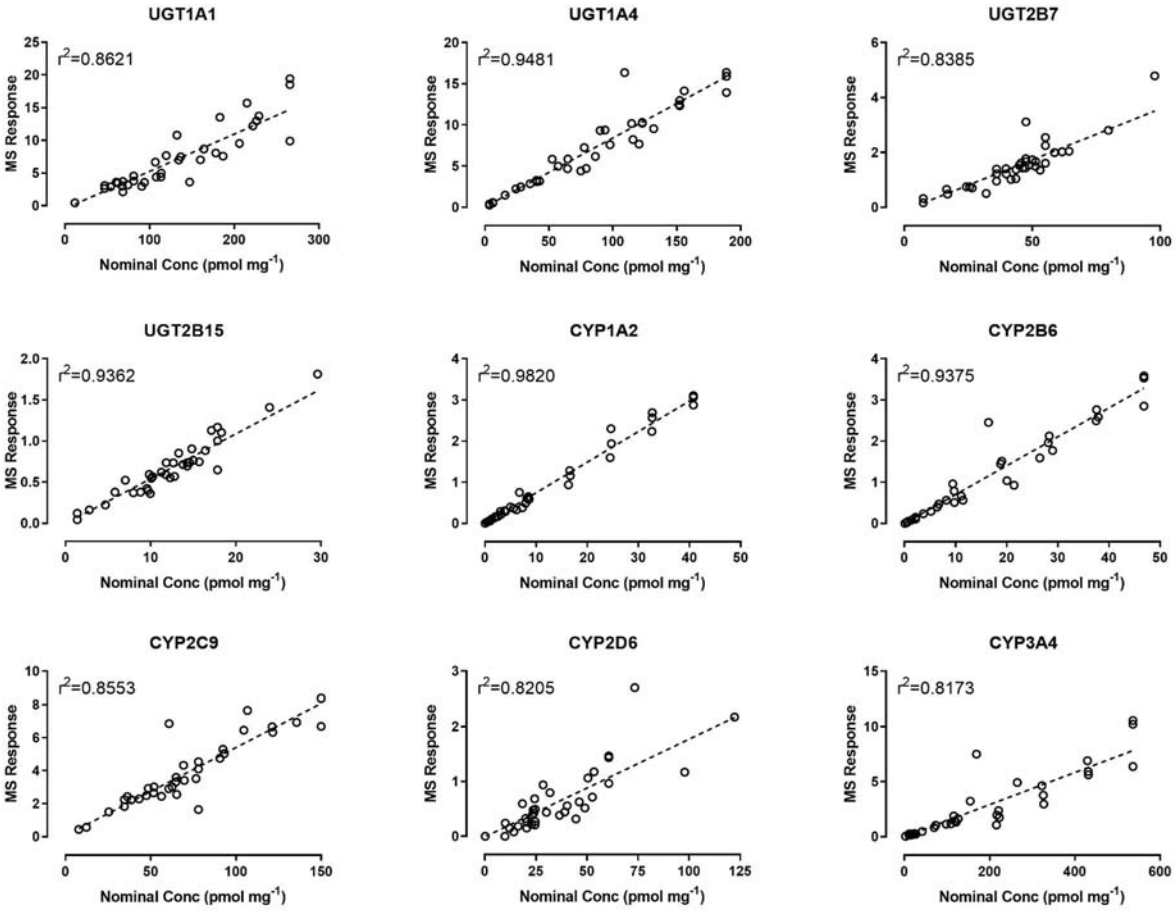

Supplemental Figure 1: Linearity plots generated with mixed HLM lots. Each plot was created using 36 mixed HLM samples. The line-of-best-fit is shown as a dotted line with the calculated correlation coefficient (r^2).

Supplemental Figure 2: Mean Relative UGT Abundances in Human Liver

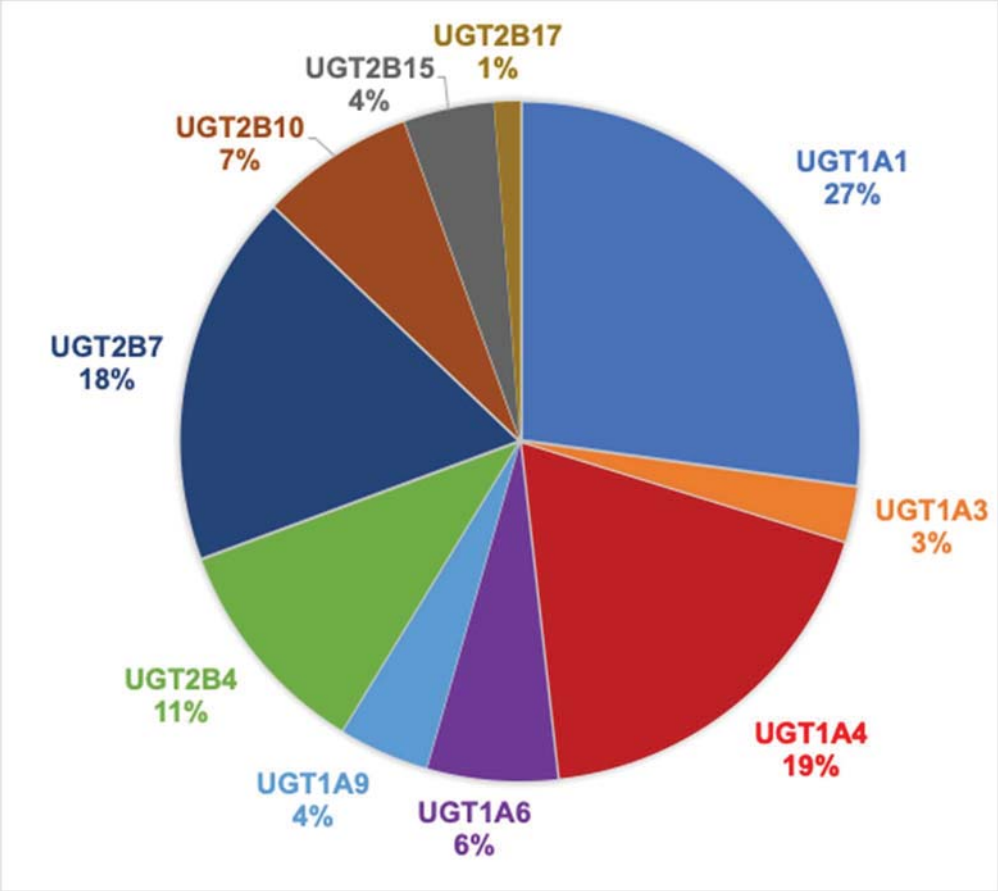

Supplemental Figure 2. The average human hepatic UGT pie. The percent contributions of individual UGT isoforms are based on the proteomics-based measurement of 130 single donor human liver microsomes.

Supplemental Figure 3: Representative LC-MS/MS chromatogram of UGT and CYP quantifier peptides